

Higgs decays into lepton pairs and a photon

Ivan Nišandžić^{a,*}

^a*Ruđer Bošković Institute, Bijenička cesta 54, 10000, Zagreb, Croatia*

E-mail: ivan.nisandzic@irb.hr

We present a new analysis of the decay processes $H \rightarrow \ell^- \ell^+ \gamma$ ($\ell = e, \mu$) which are predominantly mediated by electroweak one-loop diagrams. We derive compact and readily usable analytic expressions for the amplitude, fully reduced to scalar one-loop functions. In addition, we propose a gauge-invariant decomposition of the resonant and non-resonant contributions, which can be used for a reliable experimental extraction of the $H \rightarrow Z\gamma$ decay rate. We provide differential distributions, including the dilepton invariant mass spectrum, Dalitz plots, and forward-backward asymmetries. We also provide brief remarks on the related process $H \rightarrow \nu\bar{\nu}\gamma$.

9th Symposium on Prospects in the Physics of Discrete Symmetries (DISCRETE2024)
2–6 Dec 2024
Ljubljana, Slovenia

*Speaker

1. Introduction

Since the discovery of the Higgs boson, the ATLAS and CMS collaborations at the LHC have performed numerous analyses of its couplings, providing important probes of spontaneous electroweak symmetry breaking. While the dominant Higgs boson decay channels have been the primary focus of these measurements, recent attention has shifted towards more challenging rare decays such as $H \rightarrow Z\gamma$ [1, 2]. In this talk we present the results of a new study of the rare Higgs decay processes involving a pair of charged leptons and a photon in the final state, $H \rightarrow \ell^-\ell^+\gamma$ ($\ell = e, \mu$), based on articles [3, 4]. We also provide brief remarks on the related process $H \rightarrow \nu\bar{\nu}\gamma$, based on [5]. The observed discrepancies among previous calculations [6–8] of the differential decay width $d\Gamma(H \rightarrow \ell^-\ell^+\gamma)/dm_{\ell\ell}$ have motivated us to perform a new independent calculation of the one-loop amplitude and corresponding differential decay rates. We have performed analytic checks explicitly verifying gauge invariance, as well as ultraviolet and infrared finiteness of our results. In Ref. [3], we provide a compact expression for the amplitude, fully reduced in terms of a basic set of scalar Passarino–Veltman loop functions.

In contrast to the purely leptonic decay modes $H \rightarrow \ell^-\ell^+$, the radiative modes provide a probe of the chirality-conserving Higgs couplings to light leptons. For the electron channel, the tiny electron Yukawa coupling renders the tree-level contribution negligible, so the dominant effects arise from electroweak loop diagrams, which remain finite in the $m_e \rightarrow 0$ limit. In contrast, for the muon channel, the larger muon Yukawa coupling allows the tree-level amplitude to compete with the loop contribution¹.

These considerations define clear phenomenological goals for the $H \rightarrow \ell^-\ell^+\gamma$ decay processes. Specifically, we identify three key milestones achievable in experimental studies [4]:

1. Discovery of the process $H \rightarrow Z\gamma$.
2. Observation of $H \rightarrow \mu^-\mu^+\gamma$ at tree level driven by muon’s Yukawa coupling.
3. Search for deviations from Standard Model predictions in both $H \rightarrow Z\gamma$ and in non-resonant $H\ell^-\ell^+\gamma$ effective couplings².

We structure our phenomenological study around these objectives. In the following section, we describe the calculation of the one-loop amplitude, followed by the presentation of the differential decay rates and the separation of resonant and non-resonant contributions for the $H \rightarrow \mu^-\mu^+\gamma$ process. In Sec. 3, we briefly overview the channel with neutrinos in the final state. Finally, in Sec. 4, we briefly conclude.

2. Results

2.1 One-Loop Amplitude

Working in the linear R_ξ gauge, the one loop amplitude for the process $H \rightarrow \ell^-\ell^+\gamma$ ($\ell = e, \mu$) involves on the order of 10^2 diagrams. These can be put into three classes, namely: resonant

¹The process involving τ leptons is dominated by the tree-level contributions - this case is not discussed here.

²Possibility of new physics contributions to the effective $H\ell^-\ell^+\gamma$ coupling has recently been explored in [9, 10].

contributions $H \rightarrow Z^*(\rightarrow \ell^+\ell^-)\gamma$, contributions with the intermediate photon $H \rightarrow \gamma^*(\rightarrow \ell^+\ell^-)\gamma$, and non-resonant, box-type diagrams, as illustrated in Fig. 1.

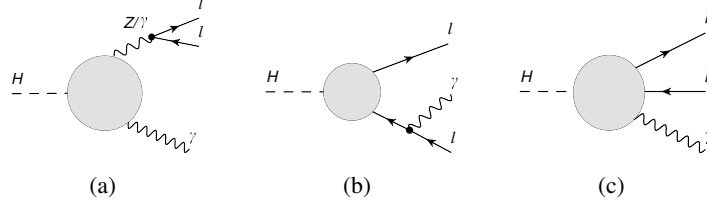


Figure 1: Classes of one-loop diagrams: (a) $H \rightarrow Z^*(\rightarrow \ell^+\ell^-)\gamma$ and $H \rightarrow \gamma^*(\rightarrow \ell^+\ell^-)\gamma$ contributions, (b, c) non-resonant box-type contributions.

Each of the individual diagram classes exhibits an explicit ξ -dependence in the linear R_ξ gauge. In particular, the ξ -dependence of the $H \rightarrow Z^*(\rightarrow \ell^+\ell^-)\gamma$ contributions cancels against that of the box and other non-resonant diagrams, ensuring gauge invariance in the total amplitude. Therefore, attempting to isolate the resonant component by taking the off-shell Z -boson vertex and multiplying it with the corresponding Breit-Wigner distribution for the Z boson leads to unphysical results [8]. This shows the necessity of gauge-invariant separation of contributions, which are discussed in Sec. 2.3 below.

We parametrize the one-loop amplitude in terms of two independent loop functions a_1, b_1 as

$$\begin{aligned} \mathcal{A}_{\text{loop}} = & \left[(k_\mu p_{1\nu} - g_{\mu\nu} k \cdot p_1) \bar{u}(p_1) (a_1 \gamma^\mu P_R + b_1 \gamma^\mu P_L) v(p_2) \right. \\ & \left. + (k_\mu p_{2\nu} - g_{\mu\nu} k \cdot p_2) \bar{u}(p_1) (a_2 \gamma^\mu P_R + b_2 \gamma^\mu P_L) v(p_2) \right] \varepsilon^{\nu*}(k), \end{aligned} \quad (1)$$

where the loop coefficients satisfy the relations $a_2(t, u) = a_1(u, t)$ and $b_2(t, u) = b_1(u, t)$, and the Mandelstam variables are defined as $s = (p_1 + p_2)^2$, $t = (p_1 + k)^2$, and $u = (p_2 + k)^2$, where p_1, p_2 , and k denote the four-momenta of the lepton, antilepton, and photon, respectively.

We performed analytic checks of the gauge invariance and the infrared and ultraviolet finiteness of our result for the amplitude. The compact expressions for the loop coefficients a_1 and b_1 are fully reduced to scalar one-loop functions and are given as auxiliary files attached to the article [3]. The corresponding results for $H \rightarrow \nu\bar{\nu}\gamma$ are found in [5]. The software packages FeynArts [11], FeynCalc [12], FeynHelpers [13], Package-X [14], and Collier [15] are employed for evaluations and cross-checks.

2.2 Differential decay rates

In Fig. 2, we show our result for the differential distributions over the invariant dilepton mass, explicitly distinguishing different contributions. The total distribution exhibits strong peaks at the Z - and the photon pole. In the muon channel, the tree-level contribution exhibits a rising behavior toward the spectrum's endpoint, competing with the loop-induced contribution. Non-resonant loop contributions are most prominent in the intermediate region between the two peaks.

Using a minimal set of kinematic cuts, detailed in [3], we obtain the branching fractions:

$$B(H \rightarrow e^-e^+\gamma) = 5.8 \times 10^{-5}, \quad B(H \rightarrow \mu^-\mu^+\gamma) = 6.4 \times 10^{-5}. \quad (2)$$

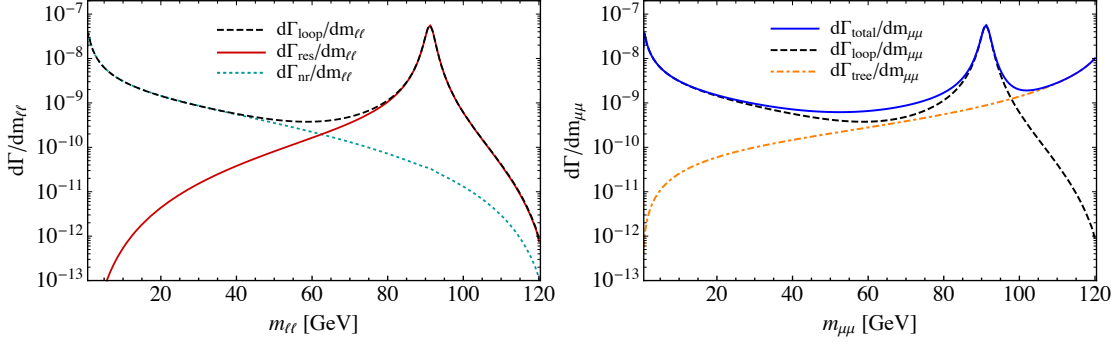


Figure 2: Differential distributions with respect to the dilepton invariant mass, with the loop contributions shown on the left, while on the right we include the tree level contribution in the muon channel.

2.3 Separation of various contributions

A detailed separation of the resonant, non-resonant, and tree-level contributions is essential for reaching the three physics goals of $H \rightarrow \ell^- \ell^+ \gamma$ decays. For this purpose, we examine the structure of the loop coefficients which take the form:

$$a_1(s, t) = \tilde{a}_1(s, t) + \frac{\alpha(s)}{s - m_Z^2 + im_Z \Gamma_Z}. \quad (3)$$

Setting $s = m_Z^2$ in $\alpha(s)$ and $\beta(s)$ isolates the gauge-invariant resonant contribution a_1^{res} from the non-resonant components:

$$a_1(s, t) = a_1^{\text{nr}} + a_1^{\text{res}}, \quad (4)$$

where³

$$a_1^{\text{nr}}(s, t) = \tilde{a}_1(s, t) + \frac{\alpha(s) - \alpha(m_Z^2)}{s - m_Z^2 + im_Z \Gamma_Z}, \quad a_1^{\text{res}}(s) = \frac{\alpha(m_Z^2)}{s - m_Z^2 + im_Z \Gamma_Z}. \quad (5)$$

This leads us to propose the following discovery strategy for the process $H \rightarrow Z\gamma$. Using the experimental data on the double differential decay width $d^2\Gamma/dsdt$, a fit to extract the quantities

$$[\alpha(m_Z^2)]^2 + [\beta(m_Z^2)]^2, \quad |a_1^{\text{nr}}|^2 + |b_1^{\text{nr}}|^2, \quad |a_2^{\text{nr}}|^2 + |b_2^{\text{nr}}|^2 \quad (6)$$

can be performed, targeting the coefficient $[\alpha(m_Z^2)]^2 + [\beta(m_Z^2)]^2 \neq 0$ at the 5σ significance⁴. This coefficient can be directly related to $\Gamma(H \rightarrow Z\gamma)$ under the narrow width approximation, as detailed in Sec. IV in Ref. [4]. To facilitate this strategy, we also provide numerical, easy-to-use expressions for the non-resonant contributions $a_{1,2}^{\text{nr}}$ and $b_{1,2}^{\text{nr}}$ in this reference.

Examining the Dalitz plots shown in Fig. 3 is instructive for formulating effective kinematic cuts to separate the various contributions. These plots show that the loop contributions are sensitive to cuts on s variable near the peaks but are relatively insensitive to the values of t and u near the phase-space edges. In contrast, the tree-level contribution peaks at low t and low u . For generic

³An analogous decomposition also applies to the loop coefficient b_1 .

⁴We note the negligible interference between resonant and non-resonant contributions.

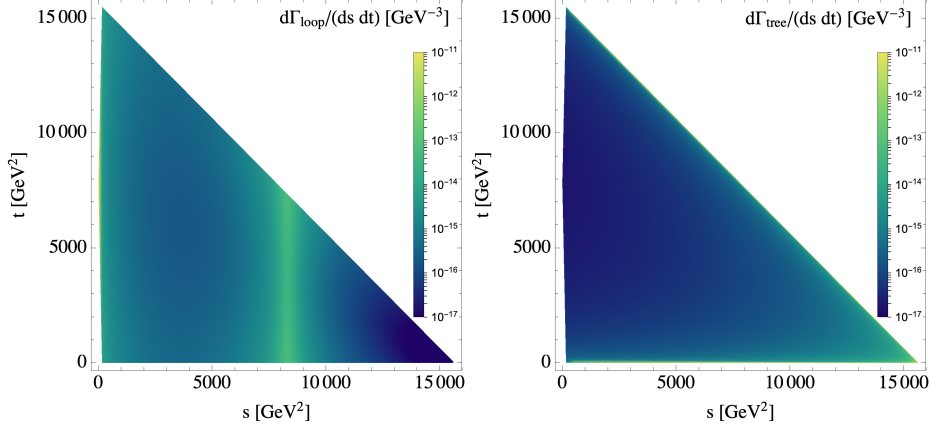


Figure 3: Dalitz plots showing the different contributions to $H \rightarrow \mu^+ \mu^- \gamma$ in the $s - t$ plane: (a) loop contributions, including both resonant and non-resonant effects, and (b) tree-level contributions.

Table 1: Integrated decay rates for different contributions to $H \rightarrow \mu^+ \mu^- \gamma$ for generic kinematic cuts on the variables s , t and u . Note the symmetric choice $\tilde{u}_{min} = \tilde{t}_{min}$.

s_{min}	s_{max}	$\tilde{t}_{min}, \tilde{u}_{min}$	$\Gamma_{res}(\text{keV})$	$\Gamma_{nr}(\text{keV})$	$\Gamma_{tree}(\text{keV})$	$\Gamma_{tot}(\text{keV})$
$(0.1 m_H)^2$	$(120 \text{ GeV})^2$	$(0.1 m_H)^2$	0.202	0.042	0.026	0.270
$(0.1 m_H)^2$	$(120 \text{ GeV})^2$	$(0.2 m_H)^2$	0.165	0.037	0.013	0.215

kinematic cuts, shown in Tab. 1, the non-resonant and tree-level contributions constitute significant fractions of the total rate.

We now outline the strategy for the separation of contributions, illustrated here for the case of the muon channel. For a resonant contribution, we focus on the region with s variable around the Z -boson peak, while applying tighter cuts on t and u variables to suppress tree-level effects. For the non-resonant contributions, we target the intermediate region between the photon and Z -peaks. For the tree-level contribution, one should keep the region with s above the Z -peak by using looser cuts on t and u .

One can further aid in the separation of tree-level and loop contributions by examining the angular distribution over $\cos \theta^{(\mu)}$, where $\theta^{(\mu)}$ denotes the angle between the charged lepton and the photon in the Higgs boson rest frame. The angular distribution turns out to be symmetric for the tree-level contribution, while the loop contribution exhibits asymmetric behavior, as shown in Fig. 4. We can therefore introduce the corresponding forward-backward asymmetry as:

$$\mathcal{A}_{\text{FB}}^{(\ell)} = \frac{\int_{-1}^0 \frac{d\Gamma}{d \cos \theta^{(\ell)}} - \int_0^1 \frac{d\Gamma}{d \cos \theta^{(\ell)}}}{\int_{-1}^0 \frac{d\Gamma}{d \cos \theta^{(\ell)}} + \int_0^1 \frac{d\Gamma}{d \cos \theta^{(\ell)}}}, \quad (7)$$

resulting in the values $\mathcal{A}_{\text{FB}}^{(e)} = 0.343$ for electrons and $\mathcal{A}_{\text{FB}}^{(\mu)} = 0.255$ for muons.

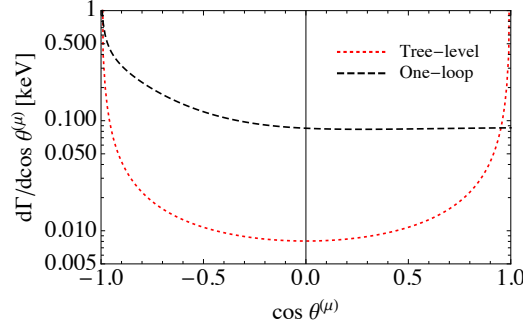


Figure 4: Forward-backward asymmetry in the angular distribution of the lepton with respect to the photon direction in the Higgs boson rest frame.

Table 2: Integrated decay rates for different contributions to $H \rightarrow \mu^+ \mu^- \gamma$ using optimized kinematic cuts on the variables s, t, u to isolate specific contributions from resonant (Γ_{res}), non-resonant (Γ_{nr}), and tree-level (Γ_{tree}) contributions.

s_{min}	s_{max}	$\tilde{t}_{min}, \tilde{u}_{min}$	$\Gamma_{res}(\text{keV})$	$\Gamma_{nr}(\text{keV})$	$\Gamma_{tree}(\text{keV})$	$\Gamma_{tot}(\text{keV})$	Purpose
$(70 \text{ GeV})^2$	$(100 \text{ GeV})^2$	$(0.1 m_H)^2$	0.195	0.002	0.007	0.204	$\Gamma(H \rightarrow Z\gamma)$
$(70 \text{ GeV})^2$	$(100 \text{ GeV})^2$	$(0.2 m_H)^2$	0.160	0.001	0.004	0.165	$\Gamma(H \rightarrow Z\gamma)$
$(10 \text{ GeV})^2$	$(40 \text{ GeV})^2$	$(0.1 m_H)^2$	$3.53 \cdot 10^{-4}$	$3.78 \cdot 10^{-2}$	$1.02 \cdot 10^{-3}$	$3.92 \cdot 10^{-2}$	nonresonant
$(20 \text{ GeV})^2$	$(40 \text{ GeV})^2$	$(0.1 m_H)^2$	$3.33 \cdot 10^{-4}$	$1.75 \cdot 10^{-2}$	$8.12 \cdot 10^{-4}$	$1.87 \cdot 10^{-2}$	nonresonant
$(100 \text{ GeV})^2$	$(120 \text{ GeV})^2$	$(0.1 m_H)^2$	$1.93 \cdot 10^{-3}$	$7.51 \cdot 10^{-5}$	$1.5 \cdot 10^{-2}$	$1.70 \cdot 10^{-2}$	tree
$(100 \text{ GeV})^2$	$(120 \text{ GeV})^2$	$(0.2 m_H)^2$	$1.40 \cdot 10^{-3}$	$5.28 \cdot 10^{-5}$	$6.06 \cdot 10^{-3}$	$7.51 \cdot 10^{-3}$	tree

3. Additional channel: $H \rightarrow \nu \bar{\nu} \gamma$

In addition to $H \rightarrow \ell^- \ell^+ \gamma$, in Ref. [5] we considered the process $H \rightarrow \nu \bar{\nu} \gamma$. In this channel, non-resonant box contributions play a significant role at high photon energies where the Z boson is off-shell. This kinematic region could provide an interesting target for experimental searches for dark sector mediators with masses below the Z boson, especially at future lepton colliders. Our result for the branching fraction

$$B(H \rightarrow \nu \bar{\nu} \gamma) = 3.2 \times 10^{-4}. \quad (8)$$

turns out somewhat lower than previous results in Refs. [16–18].

4. Conclusions

In conclusion, we have performed a new one-loop calculation for the decay process $H \rightarrow \ell^- \ell^+ \gamma$ ($\ell = e, \mu$) producing compact expressions in terms of basic scalar loop functions. We proposed a gauge-invariant separation of the resonant and non-resonant components and analyzed the kinematic cuts necessary to isolate the different contributions, thereby facilitating the extraction of $\Gamma(H \rightarrow Z\gamma)$. Our analysis suggests that detailed experimental studies of these decay channels could provide valuable insights into chirality-conserving Higgs couplings and potential deviations from Standard Model predictions.

Acknowledgments

We thank our collaborators and the DISCRETE 2024 organizing committee for the opportunity to present these results.

References

- [1] A. Tumasyan *et al.* [CMS], JHEP **05** (2023), 233 [arXiv:2204.12945 [hep-ex]].
- [2] G. Aad *et al.* [ATLAS and CMS], Phys. Rev. Lett. **132** (2024) no.2, 021803 [arXiv:2309.03501 [hep-ex]].
- [3] A. Kachanovich, U. Nierste and I. Nišandžić, Phys. Rev. D **101** (2020) no.7, 073003 [arXiv:2001.06516 [hep-ph]].
- [4] A. Kachanovich, U. Nierste and I. Nišandžić, Phys. Rev. D **105** (2022) no.1, 013007 [arXiv:2109.04426 [hep-ph]].
- [5] A. Kachanovich and I. Nišandžić, [arXiv:2405.16239 [hep-ph]].
- [6] A. Abbasabadi, D. Bowser-Chao, D. A. Dicus and W. W. Repko, Phys. Rev. D **55** (1997), 5647-5656 [arXiv:hep-ph/9611209 [hep-ph]].
- [7] Y. Sun, H. R. Chang and D. N. Gao, JHEP **05** (2013), 061 [arXiv:1303.2230 [hep-ph]].
- [8] G. Passarino, Phys. Lett. B **727** (2013), 424-431 [arXiv:1308.0422 [hep-ph]].
- [9] A. Kachanovich, J. Kimus, S. Lowette and M. H. G. Tytgat, [arXiv:2503.08659 [hep-ph]].
- [10] A. Kachanovich, [arXiv:2503.10444 [hep-ph]].
- [11] T. Hahn, Comput. Phys. Commun. **140** (2001), 418-431 [arXiv:hep-ph/0012260 [hep-ph]].
- [12] V. Shtabovenko, R. Mertig and F. Orellana, Comput. Phys. Commun. **306** (2025), 109357 [arXiv:2312.14089 [hep-ph]].
- [13] V. Shtabovenko, Comput. Phys. Commun. **218** (2017), 48-65 [arXiv:1611.06793 [physics.comp-ph]].
- [14] H. H. Patel, Comput. Phys. Commun. **197** (2015), 276-290 [arXiv:1503.01469 [hep-ph]].
- [15] A. Denner, S. Dittmaier and L. Hofer, Comput. Phys. Commun. **212** (2017), 220-238 [arXiv:1604.06792 [hep-ph]].
- [16] Y. Sun and D. N. Gao, Phys. Rev. D **89** (2014) no.1, 017301 [arXiv:1310.8404 [hep-ph]].
- [17] K. H. Phan and D. T. Tran, PTEP **2022** (2022) no.2, 023B03 [arXiv:2111.07698 [hep-ph]].
- [18] K. H. Phan, L. T. Hue and D. T. Tran, PTEP **2021** (2021) no.10, 103B07 [arXiv:2106.14466 [hep-ph]].